A "Tug of War" maintains a dynamic protein-membrane complex: MD simulations of C-Raf RBD-CRD bound to K-Ras4B at an anionic membrane

Author Affiliation:

Zhen-Lu Li[a], Priyanka Prakash[b] and Matthias Buck[a,c,d,e,1]

[a] Department of Physiology and Biophysics, Case Western Reserve University, School of Medicine, 10900 Euclid Avenue, Cleveland, Ohio 44106, United States of America

[b] Department of Integrative Biology ad Pharmacology, University of Texas Health Science at Houston, Houston, Texas 77225, United States of America.

[c] Department of Neurosciences, [d] Case Comprehensive Cancer Center as well as [e]Center for Proteomics and Bioinformatics, Case Western Reserve University, School of Medicine, 10900 Euclid Avenue, Cleveland, Ohio 44106, United States of America.

Correspondence Author: Matthias.Buck@case.edu

Keywords: K-Ras4B, small GTPase, C-Raf, Protein-Membrane Interaction, Molecular Dynamics Simulation, Potential of Mean Force.

Abstract:

Association of Raf kinase with activated Ras triggers a downstream signal cascade ending with the regulation of transcription factors in the cell's nucleus. Ras signaling has significant consequences for normal cellular function, but in some cases also for the stimulation of cancers. Accordingly, the Raf: Ras protein-protein interaction interface has been a primary target for anti-cancer drug development. However, the underlying mechanisms of the Raf: Ras interaction, particularly the contacts both proteins make with the plasma membrane, are largely unknown. Here, we present a computational study of C-Raf RBD and CRD regions (henceforth C-Raf) bound to oncogenic K-Ras4B at the membrane. The membrane is found to play an integral role in regulating the configurational ensemble of the complex by the interaction of certain regions of the K-Ras4B G-domain or the C-Raf sub-domain with anionic, phosphatidylserine lipids. Remarkably, the complex samples a few states dynamically, reflecting a competitive tug of war between C-Raf- and K-Ras4B- membrane interactions. This competition arises because the linker between the RBD and CRD sub-domains of C-Raf is short, coupled with a similar affinity of the CRD and K-Ras G-domain for the membrane, as derived by free energy calculations. This study reveals a mechanism that maintains modest binding of the overall complex at the membrane to facilitate fast signaling and one that may be common to other multiprotein, if not multidomain proteinsat membranes.

Introduction

The regulation of peripheral membrane protein function is achieved largely by the mutual interactions between the multiple proteins involved, but may be heavily influenced also by the interactions the proteins make with the membrane. While the former can be characterized in part by experiments in solution, resolving the structure of a protein complex at a membrane remains a formidable challenge experimentally given the geometrically confined regions and nature of interactions involved. Recently techniques such as electron cryo-microscopy, solution NMR with nanodiscs, and EPR/fluorescence correlation methods of proteins bound to liposomes are advancing the characterization of the interfaces, of the orientation and of the dynamics of peripheral membrane proteins at membranes (1-6). However, computational methods, such as dynamics simulations, are becoming particularly powerful in modeling the structures of proteins at membranes (7-10). In this study we apply this latter approach, to our knowledge for the first time to an aligomeric Ras – effector protein complex at a membrane.

Members of the Ras family of small GTPases, are anchored to the intracellular leaflet of the plasma membrane and are a vital regulator of cellular signal transduction: they convert the signaling input from multiple transmembrane receptors to downstream activation, typically of kinases, eventually reaching and activating transcription factors in the cell's nucleus (11). The signal transmission is achieved by the activation of Ras, converting it from Ras.GDP (inactive) to Ras.GTP (active) with the help of guanine nucleotide exchange factors, or GEF proteins. Activated Ras triggers down-stream signaling through several pathways, including the Raf-MEK-ERK cascade (12). Oncogenic mutations, which usually result in permanently activated Ras and binding to Raf, lead to severe cellular dysfunction. Importantly, ~20-30% of all human cancers harbor an oncogenic Ras mutation (13, 14). Strategies that aim to disrupt the several steps which are required for Ras activation, most notably drugs that interrupt the Raf-Ras interaction, are being developed in the recent five years and are expected to be promising therapies in cancer treatment (15-19).

Downstream effectors such as Raf and PI3K interact with Ras (20, 21). In the present investigation we studied the conformational and orientational dynamics of the C-Raf$^{RBD-CRD}$: K-Ras complex bound to membrane. That the Ras Binding Domain, or RBD (res. 56-132), makes direct contacts with the membrane-bound Ras is well established and several structures for the binding of the K-Ras4B homologous H-Ras GTPase to Raf have been presented (22, 23). There is as yet no study that clearly shows a direct interaction between Ras and the close-by Cysteine Rich Domain, CRD (res. 137-187) of C-Raf, although a number of studies have indicated such interactions (24, 25). In addition, the CRD was also identified as a membrane binding protein, especially for the lipid headgroup of phosphatidic acid (PA) and phosphatidylserine (PS) (26-28). It has long been known that in most cases membrane localization is required for Ras activity. Specifically, the membrane helps to locally concentrate Ras proteins and may direct Ras oligomerization, Ras cluster formation as well as association with other proteins, including Raf (29-31). Recent experiments as well as computer simulations have shown that the cell membrane determines the orientational preference of Ras relative to the membrane (6, 32-34), which may have an effect on the initial Raf: Ras recognition events. Despite the many studies on the interactions of isolated Raf or Ras domains with the membrane, a study of Raf: Ras as a protein complex at the membrane has not yet been reported at the molecular level.

Insights from these previous reports are employed in our study to address the following question: How are Raf-membrane, Ras-membrane and Raf-Ras interactions integrated together in order to determine the structural features and function of the Raf: Ras complex at the intracellular membrane leaflet? In the present research, computational studies provide a powerful avenue for the detailed structural and dynamic studies of the C-Raf$^{RBD-CRD}$: K-Ras4B complex at the membrane. The observations lead to the formation of further hypotheses, suggest key residues for mutagenesis for future functional studies and provide a mechanism of that can generalized to other protein complexes at membranes.

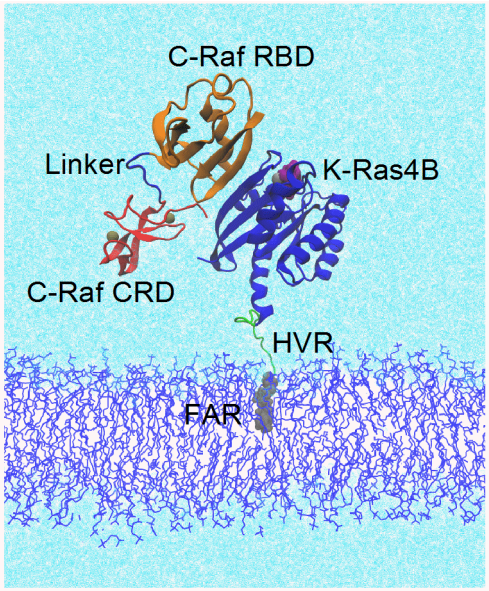

Figure 1: C-Raf$^{RBD-CRD}$: K-Ras4B complex bound to a mixed membrane containing 80% POPC and 20% POPS. The K-Ras4B protein consistes of two domains, the globular, G- or catalytic domain (res. 1-166) and the largly unstuctured hypervariable region HVR (res. 167 to 185). The C-Raf comprises the Ras Binding Domain, RBD and Cysteine Rich Domain, CRD, connected by a short linker. Proteins are shown as mainchain cartoon; Color scheme: K-Ras (blue); C-Raf: RBD (orange); CRD (red); small molecules/ions as space filling: farnesyl group (grey); GTP (purple); Zn and Mg (tan); show as lines: linker region (blue); HVR (green), membrane (blue); water (light cyan).

Results

Configurations of C-Raf$^{RBD-CRD}$

We performed five independent MD simulations of the GTPase membrane anchored complex of C-Raf$^{RBD-CRD}$: K-Ras4B for 1 μs each (Fig. 1). Before this, we first examined the configurations of an isolated C-Raf$^{RBD-CRD}$ in solution over the course of a 1 μs simulation (Fig. 2a). The configurations sampled a few major clusters (Fig. 2b-c; Fig. S1a). Overall, the CRD samples a wide configurational space relative to RBD (the figure shows a superposition on the RBD), suggesting a large flexibility of the linker between the RBD and CRD. But it is noticeable that the CRD cannot reach the β-sheet surface (β1, β2 and β5) and the region (α1 and β2) of the RBD that is used for Ras binding. Therefore, none of these C-Raf$^{RBD-CRD}$ configurations are likely to have major clashes with the binding of K-Ras. The Fusion Protein Modeller program, FPModeller (35) predicts a similarly wide configurational space of C-Raf$^{RBD-CRD}$ by rotating residues in the short linker (132 to 137) (Fig. S1b). Notably, α1 and β1, β2, and β5 regions of the RBD are also not reachable by the CRD. The interdomain linker is short, but there is also a mismatch in surface electrostatic potential between these regions and the CRD, making such configurations unfavorable. In contrast, on the other side of the proteins, there is a favorable match in

electrostatic surface potentials (Fig. 2c, lower right), and interactions between the CRD and the β3, β4 region of the RBD are occasionally established (Fig. S1c), which may contribute to high level of population of configurations that include Cluster #1 (Fig. 2b).

When bound to membrane anchored K-Ras4B, the configurational flexibility of C-Raf$^{RBD-CRD}$ is largely preserved (Fig. S2a-b). The configurations are comparable to the configurations of an isolated C-Raf$^{RBD-CRD}$, although the populations of the different configurations are changed (Fig. S2c). In addition, the radius of gyration of the C-Raf$^{RBD-CRD}$ is more extended when bound to the membrane anchored K-Ras4B (Fig. S2d). These differences reflect the additional interactions of C-Raf with K-Ras4B as well as those of C-Raf CRD with the membrane.

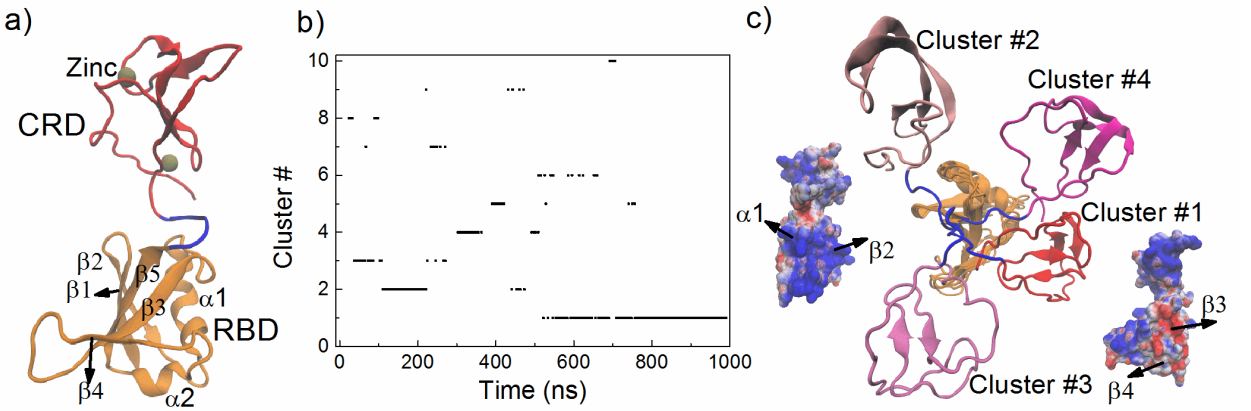

Figure 2: Configurations of C-Raf$^{RBD-CRD}$ in solution. (a) Starting configuration of C-Raf$^{RBD-CRD}$, (b) Clustering of C-Raf$^{RBD-CRD}$ configurations with an RMSD cut-off distance of 5 Å, (c) Representative configurations of the C-Raf$^{RBD-CRD}$, superimposed on RBD (pointing away from observer). Cluster #1, #2, #3, #4 are colored as red, pink, mauve, magenta. Others are shown in Fig. S1a. Left and Right side; Surface electrostatic potential of RBD and CRD, respectively showing an unfavorable interface for contacts between the domains on the front and favorable on the back.

Interaction of C-Raf$^{RBD-CRD}$ with K-Ras4B

The C-Raf: K-Ras4B interactions are mostly confined to those that are known from the C-Raf^{RBD}: H-Ras crystal structure (22), and this interface is highly persistent in the simulations. The β-sheet interface is established between residue 37-39 of K-Ras4B and residues 65-70 of the RBD (Fig. S3a). Outside these regions contacts K84:E31/D33, V88:I21/Y40 and R89:D38/S39/Y40 are seen between the RBD and K-Ras (Fig. S3a). Overall, these detailed protein-protein contacts are in close agreement with the interactions seen in the experimental structure (22). Two reports also suggested a direct interaction between the CRD and the switch II region of Ras.GTP (23, 24). These interactions are not observed, however, in the simulations (Fig. S3b). We performed one additional simulation (#6) by placing the CRD at the switch II region. However, over the course of the simulation the CRD gradually moves away from the switch II region of K-Ras4B (Fig. S3c). Experimentally, the binding of the RBD or of the CRD to Ras were measured separately. When RBD and CRD are bound together, we suggest that CRD has low potency for Ras binding, as it needs to orientate itself to a position (relative to RBD) that was not sampled in our simulation or by FPmod analysis of the isolated C-Raf$^{RBD-CRD}$ and thus is likely to be unfavorable. In a competition the RBD has a much greater advantage compared to the CRD for binding to Ras given a K_d of 20 nM versus 20 μM, respectively (36). Essentially, the CRD may be engaged in a variety of

competitive interactions amongst CRD-RBD, CRD-Ras and CRD-membrane contacts, with the latter being the most favorable.

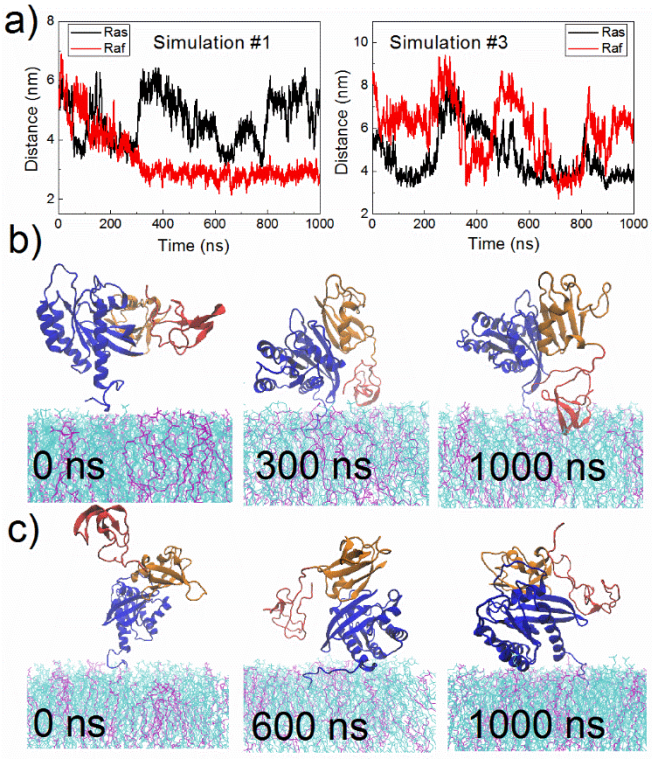

Figure 3: Dynamic membrane binding of C-Raf$^{RBD-CRD}$: K-Ras4B complex. (a) Time evolution of the distance of the center of K-Ras4B CD2 (residues 87 to 166) or the C-Raf CRD center to the membrane center. Snapshots taken at various time points from (b) simulation #1 and (c) simulation #3. Color scheme: POPC in cyan, POPS in purple; proteins (as in Fig. 1): K-Ras4B in blue, RBD in orange and CRD in red.

The K-Ras4B G-domain and the C-Raf CRD interact with the membrane in a dynamic manner

Both K-Ras4B G-domain and C-Raf CRD region are able to contact the membrane in the simulations, but, when bound together as a protein-protein complex, do so in a dynamic way. For convenience of analysis, the K-Ras4B catalytic domain (CD) is further divided into two halves, i. e, CD1 or lobe1 containing residues 1 to 86, and CD2/lobe2 with residues 87 to 166 (33, 37). Fig. 3 depicts the time evolution of the distance of the K-Ras4B CD2 or C-Raf CRD to the membrane center for simulation #1 and #3 (see Fig. S4 for others). In Fig. 3a (left), the K-Ras4B G-domain binds to the membrane for the first time during the early 100 ns, but later it undergoes a few dissociation-association events. In comparison, the CRD gradually and spontaneously moves toward the membrane in the first 400 ns, and remains bound to the membrane in the later 600 ns (Fig. 3b). In Fig. 3a (right), the K-Ras4B G-domain reaches the membrane first at ~100 ns. However, along with the movement of the CRD toward to the membrane at ~350 ns, the K-Ras4B G-domain then moves away from the membrane. Later, the positions of both K-Ras4B and CRD undergo several fluctuations (Fig. 3c). Simulations #2, #4 and #5 show a range of similar scenarios to these two (Fig. S4). Overall, the membrane contacts of K-Ras4B or CRD are not highly persistent but are dynamic in nature. This differs from the situations when isolated K-Ras4B (and also -4A) are placed

at a membrane with the same concentration of POPS lipid molecules, where K-Ras is mostly bound to the membrane, detaching less frequently (32, 33).

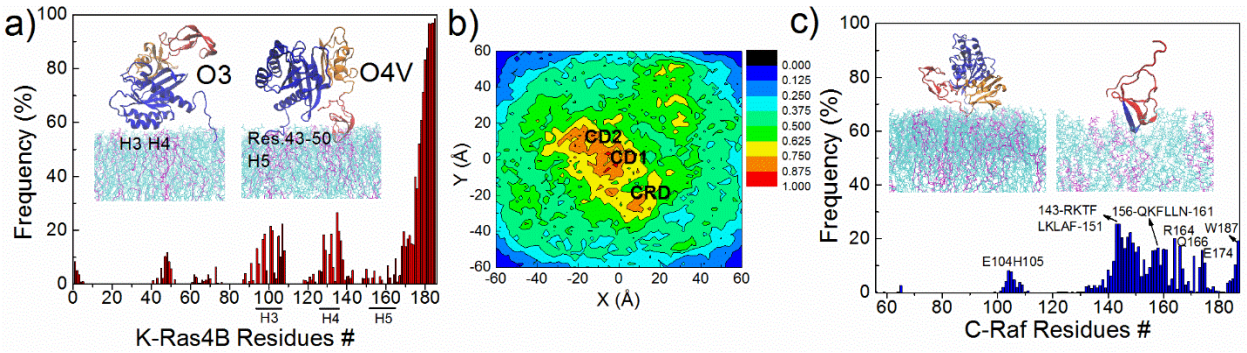

Figure 4: Interface of the K-Ras4B: membrane interaction. (a) Frequency of membrane contacts for residues of K-Ras4B; position of helices 3-5 is indicated. Residues within 5 Å of the membrane surface are treated as membrane contact residues. Inset images show major orientations of K-Ras4B relative to the membrane. (b) POPS distribution at the membrane. The distribution is normalized to make the maximum equal 100%. K-Ras4B CD1 is centered at (0, 0), the horizontal displacement between the center of mass of K-Ras4B CD1 and that of C-Raf RBD is aligned to the X axis. (c) Frequency of membrane contacts for residues of C-Raf. Position of membrane interacting region, res. 143-150 is indicated in blue. Inset images: Representative domain orientations of the RBD and CRD relative to the membrane.

Interface of K-Ras: membrane interaction

Residues involved in contacting the membrane are plotted in Fig. 4a and Fig. 4b for K-Ras4B and C-Raf separately as a function of sequence and as averaged over the 5 simulations. Regarding the G-domain of K-Ras4B, the membrane interacting residues belong mostly to helix 3 and helix 4, less so to helix 5 and a small loop segment between β2 and β3 (residues 43-50, loop 3). These interface residues correspond to the two dominant orientations of K-Ras at the membrane (O3 and O4V; see also Fig. S5). In one orientation, helix 3 and 4 are bound to the membrane; in the other one, the loop 3, and less helix 5 are the membrane interacting residues. For an isolated K-Ras, O3 and O1 orientation (where β1-β3 associates with the membrane) are the dominant orientations (32, 33). When bound to C-Raf, the O1 orientation is completely abolished, as the corresponding β1-β3 interface of K-Ras is now strongly bound to C-Raf. Therefore, O3 becomes the dominant orientation for K-Ras in complex with C-Raf at the membrane. Additionally, the membrane association of the CRD, in some cases, also brings the K-Ras loop 3 close to the membrane, resulting in the popularity of O4V. O4V is a variant of a previously characterized orientation, O4 (where not only the loop 3, but also helix 4 and 5 are largely involved in membrane contacts). A cluster of anionic POPS lipid molecules is apparent under and around the C-Raf: K-Ras4B complex (especially under the GTPase, Fig. 4b). Clustering of anionic POPS lipid molecules is expected to enhance the binding of K-Ras to the membrane, similar to previous studies (32, 33).

Interfaces for the C-Raf: membrane interaction

As for C-Raf, only a few residues of the RBD (residues 56 to 132) can contact the membrane (Fig. 4c). But the RBD-membrane contact frequency is rather low with the largest occupancy about 8.1% and 7.7% for E104 and H105 separately. The most prominent membrane contacts involve residues in the CRD.

Almost all of the residues in the CRD (residues 137 to 187) are able to contact the membrane more or less equally, except for a few residues hidden inside the folded conformation such as residues around V180 (Fig. 4c). The CRD-membrane interaction is driven by both hydrophobic and by electrostatic contacts. The CRD can become partially buried into the membrane (most notably in simulation #1), with hydrophobic residues L147, L149, L159 and L160 largely buried into the membrane. The same region is also predicted as membrane inserted by the OPM (Orientations of Proteins in Membranes) webserver (38). Positively charged residues including R143, K144, K148, K157 and R164 also interact with the lipid bilayer, which is consistent with the experiment-based report that the 143-RKTFLKLA-150 segment of the CRD has a role in membrane binding (27). In addition, cation-π interactions established between F146, F158 and especially F151 and W187 and the Nitrogen of the lipid headgroup (Fig. S6a), as well as hydrogen bonding interactions between residues T145, Q156, N161 (Fig. S6b) also aid the membrane adhesion of the CRD.

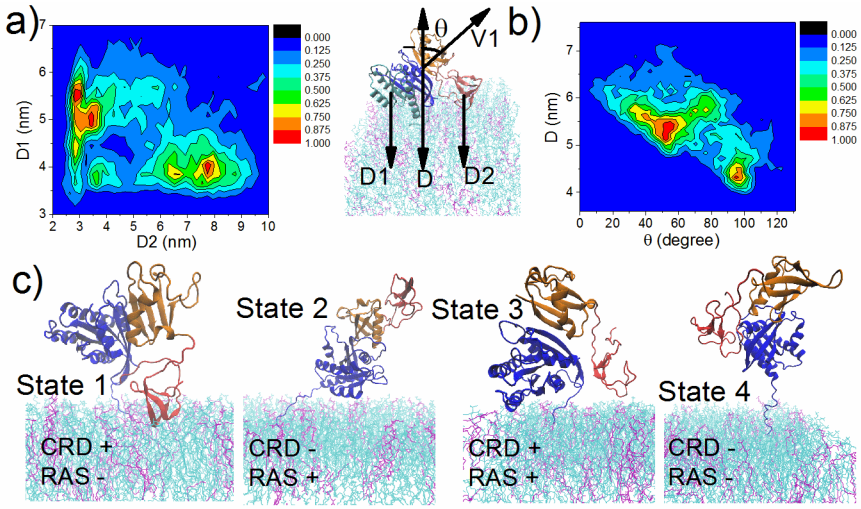

Figure 5: Configurations of the C-Raf: K-Ras4B complex at the membrane. The variables are defined as follows: D1 is distance of K-Ras4B CD2 to the membrane center; D2 is the distance of CRD to the membrane center. D is distance between the center of the RBD: K-Ras4B^{CD1} and center of the membrane. V1 is a vector connecting the center of K-Ras4B CD1 to the center of RBD. θ is the cross angle between vector V1 and the normal direction of membrane surface. K-Ras4B CD1, CD2, RBD, CRD in cyan, blue, orange and red respectively. (a) Contour maps plotted with variables D1 versus D2. (b) Contour maps with variables D versus θ. (c) Representative configurations for the 4 possible states of C-Raf: K-Ras4B complex.

Configurations of the C-Raf$^{RBD-CRD}$: K-Ras4B complex at the membrane

The configurations of the C-Raf: K-Ras4B complex with respect to the lipid bilayer are further characterized using several geometric parameters as shown in Fig. 5. In Fig. 5a, the distance of the K-Ras4B catalytic subdomain (CD2) to the membrane center is plotted versus the distance of the CRD to the membrane center. In one dominant conformation the CRD is away from the membrane and the K-Ras4B CD2 is bound to the membrane (distances of ~8 nm and ~4 nm respectively). In contrast, another dominant conformation corresponds to CRD approaching the membrane and CD2 pointing away from it (distances ~3-3.5 nm and ~5-5.5 nm, respectively). Otherwise, there are instances when none of the domains are in contact with the membrane and times when both the K-Ras4B G-domain and C-Raf CRD regions are close to the membrane (~3.5 nm, 3.7nm, respectively), although such instances are rare. Fig. 5b plots another pair of parameters that characterize the relative position and orientation of the RBD

and the K-Ras4B CD1 regions. Again, two orientations dominate---one with the RBD: K-Ras4B^{CD1} centered at ~5.3 nm from the membrane center and with the RBD slant upward (tilt angle centered at ~54°); another represents a position tilted at around 95° and is centered at ~4.2 nm. Unbound states can also be identified at where the RBD: K-Ras4B^{CD1} is far away from the membrane and almost being parallel with the membrane surface. Overall, we classify the well populated configurations of the C-Raf: K-Ras4B complex at the membrane into four states. Representative conformations for these four states are shown in Fig. 5c. The first two states (CRD+/RAS- and CRD-/RAS+) represent the most dominant configurations for the complex.

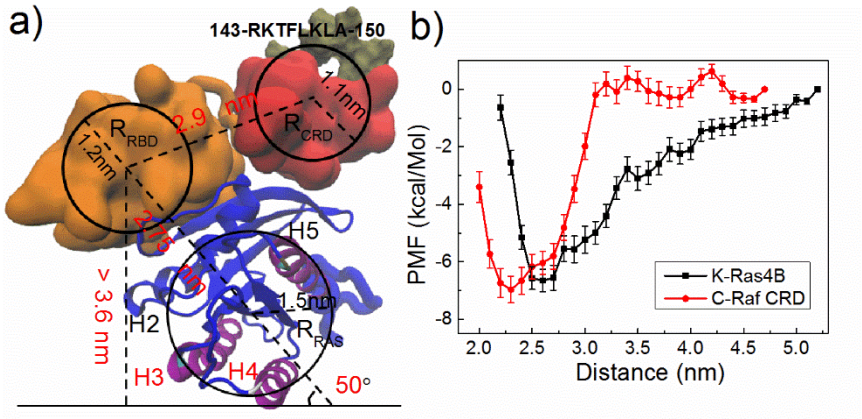

Figure 6: Tug of War between K-Ras4B and C-Raf CRD membrane interactions. (a) Schematic picture of steric position (geometric limitations) of K-Ras4B and C-Raf complex in different states (here State 2; SI Fig. S5, state 1). (b) Potential of mean force, PMF, for K-Ras4B and CRD binding to the model membrane. Error bars were estimated from a Monte Carlo bootstrap analysis.

Mechanism of non-cooperativity between CRD and K-Ras4B-membrane interactions

It is apparent that the CRD and K-Ras4B G-domain contact the membrane mostly in a mutually exclusive manner. The non-cooperative mechanism is largely determined by the geometric feature of C-Raf$^{RBD-CRD}$: K-Ras4B complex. We have identified the most favorable membrane interaction interfaces as residues 143-RKTFLKLA-150 for the CRD and helix 3 and 4 for K-Ras4B, respectively. However, when helix 3 and helix 4 of K-Ras4B contact the membrane, the RBD as the counterpart of K-Ras4B is moved away from the membrane with a slant angle at ~50 degree (Fig. 6a). The calculated radius of gyration for K-Ras CD, RBD, and CRD are 1.5, 1.2 and 1.1 nm respectively (the physical radius is even slightly larger). The distance between center of K-Ras CD and RBD is about 2.75 nm and between center of RBD and CRD is averaged at 2.9 nm. Based on the slant angle and the size of these sub-domains, the RBD is at least 3.6 nm away from the membrane surface. Although CRD has large freedom to adopt multiple orientations relative to the RBD, none of them enable the CRD to reach the membrane without rotating the K-Ras domain, as the maximal length of the linker plus the CRD is estimated at 2.8 nm (2.9-1.2+1.1 nm, Fig. 6a). Therefore, the most favorable membrane-associated state for CRD and K-Ras4B cannot coexist. Fig. S7 further discusses the opposite situation when CRD is bound to the membrane. Overall, the C-Raf: K-Ras4B complex may either use 143-RKTFLKLA-150 of CRD (state 1) or alternatively use helix 3 and helix 4 of K-Ras4B (State 2) to interact with the membrane. This effectively reflects a tug of war between these two interactions.

Free energy of K-Ras4B and C-Raf CRD membrane adhesion

We further estimate the binding affinity of K-Ras4B and C-Raf CRD to the model membrane by calculating the potential of mean force (PMF) along a path of membrane (un-)binding using the most favorable domain orientations (Fig. 6b, see Method). The calculated PMF is -6.57 kcal/Mol for K-Ras4B.G12D binding to the model membrane. The simulation results are comparable to our microscale thermophoresis (MST) experiments, where the K_d was measured at 23.4 μM (ΔG = -6.31 kcal/Mol) at 298 K for K-Ras4B.G12V binding to a membrane comprised of POPC and 5% PIP2 molecules (Manuscript in preparation). The calculated PMF is -6.97 kcal/Mol for the CRD binding to the membrane. The value is close to value predicted via OPM sever (-7.31 kcal/Mol). Both of these energies correspond to a medium binding affinity toward to the membrane, and since the CRD- and K-Ras4B-membrane interactions are mostly competitive, none of these two domains have an overwhelming advantage in membrane adhesion. Together with the geometric set-up of the domains this explains the balance in the tug-of war interplay between CRD- and K-Ras4B-membrane interactions.

DISCUSSION

Structural preferences and dynamics of protein complexes at membranes are still a relatively new terrain for discovery. The field has been hampered by the experimental challenges involved, but techniques, especially computational methods are recently emerging. In this study, we chose one complex as an example and performed multiple μs molecular dynamics simulation for C-Raf$^{RBD-CRD}$ bound to K-Ras4B at the membrane. While several studies have examined the orientation and dynamics of isolated K-Ras at the membrane (6, 32-34), there are as yet no simulations of C-Raf: K-Ras at membranes. Our study presents a first step towards understanding the configuration and dynamics of this assembly, where C-Raf is considered as a multi-domain protein with the inclusion of its RBD and CRD domains. While no experimental structural or biophysical data is available at present for such a C-Raf multidomain protein construct, our study, importantly, predicts a novel competitive mechanism between membrane adhesion of K-Ras4B G-domain and C-Raf CRD of the protein complex (Fig. 5). We are able to rationalize the behavior of this system by considering both the geometric features of the domains within the complex (Fig. 6a) as well as a by the estimation of a comparable binding affinity between the two subunits and the membrane (Fig. 6b).

The results from the simulations have several implications for the biological function of the Raf : Ras system: A relatively tight Ras: Raf association was reported with a K_d of 20 nM (36). The K_d for Ras G-domain membrane binding and Raf CRD-membrane interactions were measured at ~20 μM in our simulations. Thus, the membrane binding of the K-Ras4B G-domain and of the C-Raf CRD by themselves are only marginally strong. One might expect that additional interactions, such as possible direct interaction of the C-Raf CRD and K-Ras4B domains would substantially increase this affinity via synergistic effects. In fact, this is frequently seen with cell signaling proteins, such as the interactions between WASP, Cdc42 and the membrane, which utilize multiple interactions in a cooperative manner to maximize the signaling output while minimizing output in the absence of coincident input signals (39, 40). However, this is not the mechanism predicted by our simulations and free energy calculations here. Instead, we suggest that an intrinsically weak association gives K-Ras more freedom to interact with

multiple regulatory and effectors proteins, which we believe could have a role in the biological function of K-Ras4B.

The study also confirms that the orientation state (O1), that was previously identified as the dominant state of isolated K-Ras.GTP relative to the membrane (32, 33), is indeed occluded for Raf-binding and may not be sampled significantly in a cellular environment, given the tight binding between C-Raf RBD and K-Ras (also supposing a high abundance of C-Raf). It is possible that over a long period of time, the structures of K-Ras and the C-Raf RBD may adjust at the membrane to weaken this interaction. However, the fact that the residues involved in this protein-protein interaction as well as the G-domain and CRD–membrane contacts are highly conserved speaks against this scenario and suggests that the competitive interactions are qualitatively similar. Specifically all K-, H and N-Ras are sequence invariant for the first 86 residues, parts of which comprise the contact region with the RBD; on the side of the RBD, res. 65-70 as well as K84, R89 are identical between B- and C-Raf (V88 is changed to M in B-Raf); the region of residues 143-150, primarily responsible for membrane interactions is also conserved. The extent of conservation of Ras–membrane interaction sites is also high across the Ras G-domains (41). Using the knowledge derived from the present study we may speculate how the Raf: K-Ras interaction may be blocked therapeutically. The Raf binding site on K-Ras is well localized and the interaction is tight. While the association could be weakened by trapping Ras in a membrane-associated state that is not compatible with this mode of C-Raf RBD binding to the GTPase (32, 33), the binding of Ras to the membrane in such an orientation state would need to be considerably enhanced by designing molecules that mediate the Ras-membrane interactions.

The binding of C-Raf to a membrane anchored K-Ras4B results in a complex that continues to sample multiple states with respect to the membrane in a dynamic mannner. The optimal K-Ras4B and C-Raf CRD – membrane bound states present alternative orientations of the overall complex, i.e., membrane contacts of one of them will exclude the best membrane contacts of the other, reflecting a “Tug of War” between membrane interactions of K-Ras4B and C-Raf CRD. This keeps the binding affinity in the modest range, typically associated with cell signaling processes, which also means that interactions are kinetically labile and quick to switch off. It should be noted that the interactions and the balance in the “Tug of War” may likely be tuneable by altering the binding affinity of of the individual domains with the membrane. For example, we recently predicted that a PIP2 containing membrane leads to more defined/less dynamic states of K-Ras4A, suggesting that the strength of interaction between the G-domain of the GTPase and the membrane are increased (33).

It is accepted that Ras activity in cells requires its localization to the membrane. Ras clustering is an undisputed observation (29-31), but the role of G-domain contacts in Ras dimerization in solution and at the membrane is not yet clear. Recently, symmetric Ras: Ras dimers have been predicted through molecular docking, although they mainly represents a weak association (K_d ranges from 1 μM to greater than mM) (42, 43). Conformational state 2 of C-Raf: K-Ras4B predicted in our simulations does not match with any of predicted dimer forms of Ras (Fig. 5c). But state 1 is suitable for the formation of Ras dimers, due to the increased exposure of helix 3 and 4 of K-Ras4B (Fig. 5c) which comprise the dimer interface (42, 43). However, in this case optimal G-domain membrane binding and K-Ras dimerization would also oppose one another. Nevertheless, CRD-membrane interactions may help to orient the GTPase at the membrane for improved dimerization kinetics, and depending on K-Ras vs. C-Raf concentration,

could stimulate K-Ras dimer formation. We are currently working on modeling possible higher order C-Raf : K-Ras complexes, but the added complexity of this system is beyond the scope of this report.

Similarly, we can only speculate at present, how the C-Raf$^{RBD-CRD}$: K-Ras4B configurations observed in this study may affect the activation of C-Raf Kinase Domain (KD). The auto-inhibition of C-Raf is achieved through blocking the KD by direct interactions with the RBD-CRD region (44). The RBD: Ras.GTP recognition and possibly also the membrane adhesion of the CRD likely help to unlock the auto-inhibition of C-Raf, resulting in an open conformation of C-Raf KD necessary for KD dimerization. This dimerization is thought to be a critical step for kinase activity. Based on the findings here, once recognition between K-Ras4B and C-Raf RBD is established, the CRD can reorient and may be at least partially inserted into the membrane (Fig. 3). This structural rearrangement is related to the steric distribution of the hinge/loop region that connects the KD and the RBD-CRD domains; however this region is rather long and likely flexible (res. 185 to 349).

Finally, the findings of our study also have general implications for cell signaling involving protein complexes at the cellular membrane. From other examples of membrane anchored and peripheral membrane proteins it is becoming clear, that the membrane actively participates in the regulation of peripheral membrane protein function (1-10). However, the membrane-protein interactions typically synergize to compete with protein-protein interactions. For example, the membrane adhesion of Scaffold protein-Ste5, could release the auto-inhibition of itself caused by intramolecular interaction between two domains (45). Another example is the Focal Adhesion Kinase, FAK system, where both kinase and FERM domains can interact with PIP2 in membranes, leading to a dissociation of these two regions, then allowing the kinase domains to dimerise and activate (46). However, specifically, a "Tug of War" mechanism has been known in biology in the release cycles by chaperones and in the cargo transport through motor proteins (47, 48). Now we have found an example of a mechanism involving a membrane peripheral protein complex involved in competition by virtue of its interactions with the membrane. Overall, these processes are achieved through coordination of interactions amongst multiple proteins and the interactions of protein subunits/domains with the membrane. The study here reveals these coordination mechanisms at molecular level, laying the foundation for unveiling complicated signal process through peripheral membrane proteins.

Method

Method Summary

The model of C-Raf$^{RBD-CRD}$ was built by connecting the crystal structures of the C-Raf RBD (PDB, 4G0N) (22) and C-Raf CRD (PDB, 1FAQ) (26) with the native linker. The C-Raf$^{RBD-CRD}$: K-Ras4B complex was further built by docking the modeled C-Raf$^{RBD-CRD}$ structure and to the crystal structure of K-Ras4B (PDB, 4DSO), based on the crystal structure of H-Ras bound with the C-Raf RBD (PDB, 4G0N) (22). The system was placed at a membrane containing 80% POPC and 20% POPS. Five independent simulations were performed each for 1 μs. Umbrella sampling simulations were performed to calculate the free energy of CRD and K-Ras4B binding to the membrane. The CHARMM36m force field was used in all simulations and energy calculations (49). Details of the model construction, molecular simulation, free energy calculation and analysis are shown as below.

Starting model: C-Raf$^{RBD-CRD}$ in solution

The structure of the C-Raf$^{RBD-CRD}$ complex was established by assembling the separately available crystal structures of the C-Raf RBD (PDB, 4G0N) and C-Raf CRD (PDB, 1FAQ) using a flexible linker with the protein sequence of residues 133-136 that links these two domains. The C-Raf RBD and C-Raf CRD are connected using the webserver AIDA, where it links the protein subdomains together by addressing the relative orientation between RBD and CRD (50). The predicted structure was then used as starting configuration of C-Raf (denoted, SC0) was examined by a 1.0 μs simulation in solution. There are two zinc fingers in C-Raf CRD. Each zinc finger has one zinc ion surrounded by three Cysteine residues and one Histidine residue. Histidine is in the uncharged HSE form and Cysteine is patched with CYN (51). The ion coordination within the Zinc finger was stable in all simulations.

C-Raf$^{RBD-CRD}$: K-Ras4B complex at the membrane

The modeled C-Raf$^{RBD-CRD}$ structure (above) was further combined with K-Ras4B (PDB, 4DSO) to construct the initial C-Raf$^{RBD-CRD}$: K-Ras4B complex, guided by a crystal structure of H-Ras bound with RBD (PDB, 4G0N) (22). We carried out 6 independent simulations for the complex, named as Simulation #1 to #6 (see Table S1). In Simulation #1-#4, the center of mass of the catalytic domain of K-Ras4B was placed ~6 nm away from the center of x-y membrane bilayer plane in the Z direction. In Simulation #5, an effector-interacting orientation of K-Ras (where helix 3 and helix 4 are in direct contact with the membrane) was used as the starting structure (32, 33). In Simulation #1, #2 and #5, the starting configurations of C-Raf$^{RBD-CRD}$ was that of SC0 (see section above). In Simulation #3 and #4, two other different configurations extracted from the 1 μs simulation of C-Raf in solution were adopted. In this way, the initial displacement of CRD relative to the membrane could be larger (~8.5 nm, Simulation #3) or smaller (~5 nm, Simulation #4) than in Simulation #1 and Simulation #2 (~6 nm). In addition, one simulation, #6, was carried out by placing the CRD at the switch II region of K-Ras to test whether this proximity leads to the formation of stable contacts. This simulation was performed for only 240 ns. In all simulations K-Ras4B G-domain was linked to the HVR and anchored to the membrane with a C-terminal farnesyl group pre-inserted into the membrane following previous studies (32, 33). The parameters for the farnesyl group were generated by the CHARMM generalized force field (CGenFF) (52). The model membrane was composed of 360 POPC (Palmitoyloleoyl-phospatidyl-choline) and 90 POPS (1-Palmitoyl-2-oleoylphosphatidylserine) lipid molecules (20 % POPS). The POPS are equally distributed

in each leaflet of the membrane. All model membranes were created by the CHARMM-GUI and equilibrated for 100 ns (53).

Simulation Conditions

The modeled structure of C-Raf$^{RBD-CRD}$: K-Ras4B complex was solvated in a box of TIP3P water. A number of water molecules were replaced randomly by Sodium and Chloride to obtain a neutral charge system with a near-physiological ion concentration of 150 mM. The simulation systems were energy minimized for 2000 steps. Sequentially, a short simulation of 0.5 ns was performed with a harmonic restraint on protein heavy atoms and lipid phosphate groups, followed by another 0.5 ns restraint simulation on only the Cα atoms of the proteins. Production simulations were carried out for 1 μs for Simulation #1 to #5 of the modeled C-Raf$^{RBD-CRD}$: K-Ras4B complex. The initial 50 ns of all simulations were performed using the NAMD/2.10 package (54). The NAMD simulations were performed with a time step of 2 fs, and were coupled with a thermostat at 310 K, and a barostat at 1 bar with a semi-isotropic Langevin scheme. The equilibrated NAMD simulations were converted to Anton2---a specialized supercomputer for molecular dynamics simulation (55), for the remaining 950 ns simulation.

Free Energy Calculations

In order to calculate the potential of mean force (PMF) of K-Ras4B or C-Raf CRD binding to the membrane, umbrella sampling simulations were performed (56). The reaction coordinate is set as the distance in the Z direction between the center of mass of the model membrane and the center of the mass of K-Ras4B helix 4 (residues 127 to 137), or the center of mass of a previously identified lipid binding loop (residues 143 to 151) of the CRD. The membrane is composed of 176 POPC and 44 POPS lipid molecules. The relative orientation of K-Ras4B is set with the helix 4 axis facing the membrane, and CRD is placed with the 143-RKTFLKLAF-151 segment also in parallel facing the membrane. Umbrella windows with a 0.1 nm interval were extracted from the simulation trajectories of two steered molecular dynamics (SMD) simulations. K-Ras4B was pulled from a position 5.2 nm distant from the membrane center to the membrane surface (Z = 2.2 nm), and CRD was pulled from a pre-inserted position (Z = 2.0 nm) to a non-membrane associated position (Z = 4.7 nm). A constant pulling velocity of 10^{-7} nm per time step (1fs) was used (total 30-40 ns SMD simulations). Biased simulations were performed with a harmonic potential applied between the protein Cα atoms and the membrane with a force constant of 10 kcal/(Mol.$Å^2$). For K-Ras4B, the sampling simulations were performed for each window for 12 ns. For CRD, sampling simulations were applied for each window for 20-40 ns. The last 10 ns of umbrella sampling trajectory were used in order to calculate the PMF, with the application of the weighted histogram analysis method (WHAM) (57).

Analysis

Unless stated otherwise, we performed all our analysis based on the Anton simulations (950 ns) after excluding the initial 50 ns from each trajectory as equilibration. The trajectories of C-Raf$^{RBD-CRD}$ were clustered using Wordom (Fig. 1) (58). Fusion Protein Modeller (34) was used to explore the configurational space of C-Raf$^{RBD-CRD}$ by rotating residues in the shorter linker (132 to 137) (Fig. S1b). The contact maps between one protein domain with another (RBD: CRD, RBD: RAS, CRD: RAS) were made by counting the contact events, i.e. when the distance between residues of one domain and residues of another domain is less than 5.0 Å. Occupancy is the % number of simulation frames where the interaction is present (Fig. S1c and Fig. S3). The criteria for a cation-π interaction is that the distance

between all the aromatic ring atoms and the choline nitrogen are below 7 Å and that there is no more than a 1.5 Å in difference between these distances (Fig. S6). For presence of hydrogen bonds a distance of 3.5 Å and angular cut-off of 30 degree was used.

Author contribution

Z.L.L. and M.B. conceived and designed the study with P.P contributing simulation #6; Z.L.L. and P.P. performed the simulations; Z.L.L., P.P. and M.B. analyzed the data; Z.L.L., P.P. and M.B. wrote the manuscript.

Acknowledgement

This work is supported by NIGMS grant R01GM112491 to the Buck lab.; P. Prakash is supported by Cancer Prevention and Research Institute of Texas (CPRIT No. DP150093). We thank A.A. Gorfe for helpful discussion and the Ohio Super Computer center located in Columbus, Texas Advanced Computing Center (TACC) and the Extreme Science and Engineering Discovery Environment (XSEDE; Project: MCB150054) for computational resources. Anton2 Computer time was provided by the Pittsburgh Supercomputing Center (PSC) through Grant R01GM116961 from the National Institutes of Health.

References

1. Denisov IG, Sligar SG (2016) Nanodiscs for structural and functional studies of membrane proteins. *Nat Struct Mol Biol* 23:481–486.
2. Zorman S, Botte M, Jiang Q, Collinson I, Schaffitzel C (2015) Advances and challenges of membrane–protein complex production. *Curr Opin Struct Biol* 32:123-130.
3. Calvez P, Schmidt TF, Cantin L, Klinker K, Salesse C (2016) Phosphatidylserine allows observation of the calcium–myristoyl switch of recoverin and its preferential binding. *J Am Chem Soc* 138: 13533–13540.
4. Pérez-Lara Á, Thapa A, Nyenhuis SB, Nyenhuis DA, Halder P, Tietzel M, Tittmann K, Cafiso DS, Jahn R (2016) PtdInsP2 and PtdSer cooperate to trap synaptotagmin-1 to the plasma membrane in the presence of calcium. *eLife* 5:e15886.
5. Ye X, McLean MA, Sligar SG (2016) Phosphatidylinositol 4,5-bisphosphate modulates the affinity of talin-1 for phospholipid bilayers and activates its autoinhibited form. *Biochemistry* 55:5038-5048.
6. Mazhab-Jafari MT, Marshall CB, Smith MJ, Gasmi-Seabrook GM, Stathopulos PB, Inagaki F, Kay LE, Neel BG, Ikura M (2015) Oncogenic and Rasopathy-associated K-Ras mutations relieve membrane-dependent occlusion of the effector binding site. *Proc Natl Acad Sci USA* 112:6625-6630.
7. Gorfe AA, Hanzal-Bayer M, Abankwa D, Hancock JF, McCammon JA (2007) Structure and dynamics of the full-length lipid-modified H-Ras protein in a 1,2-dimyristoylglycero-3-phosphocholine bilayer. *J Med Chem* 50:674-684.
8. Yamamoto E, Kalli AC, Yasuoka K, Sansom MSP (2016) Interactions of pleckstrin homology domains with membranes: adding back the bilayer via high-throughput molecular dynamics. *Structure* 24:1421–1431.
9. Grauffel C, Yang B, He T, Roberts MF, Gershenson A, Reuter N (2013) Cation−π interactions as lipid-specific anchors for phosphatidylinositol-specific phospholipase C. *J Am Chem Soc* 135:5740–5750.
10. Ryckbosch SM, Wender PA, Pande VS (2017) Molecular dynamics simulations reveal ligand-controlled positioning of a peripheral protein complex in membranes. *Nat Commun* doi:10.1038/s41467-016-0015-8
11. Simanshu DK, Nissley DV, McCormick F (2017) RAS proteins and their regulators in human disease. *Cell* 170:17-33.
12. Vetter I, Wittinghofer A (2001) The guanine nucleotide-binding switch in three dimensions. *Science* 294:1299-1304.
13. Prior IA, Lewis, PD, Mattos CA (2012) A Comprehensive survey of Ras mutation in cancer. *Cancer Res* 72:2457-2467.
14. Schubbert S, Shannon K, Bollag G (2007) Hyperactive Ras in developmental disorders and cancer. *Nat Rev Cancer* 7:295-308.
15. Welsch ME, Kaplan A, Chambers JM, Stokes ME, Bos PH, Zask A, Zhang Y, Sanchez-Martin M, Badgley MA, Huang CS, Tran TH, Akkiraju H,Brown LM, Nandakumar R, Cremers S, Yang WS, Tong L, Olive KP, Ferrando A, Stockwell BR (2017) Multivalent Small-Molecule Pan-RAS Inhibitors. *Cell* 168:878-889.

16. Athuluri-Divakar SK, Vasquez-Del Carpio R, Dutta K, Baker SJ, Cosenza SC, Basu I, Gupta YK, Reddy MV, Ueno L, Hart JR, Vogt PK,Mulholland D, Guha C, Aggarwal AK, Reddy EP (2016) A small molecule Ras-mimetic disrupts Ras association with effector proteins to block signaling. *Cell* 165:643-655.
17. Ostrem, JM, Peters U, Sos ML, Wells JA, Shokat KM (2013) K-Ras (G12C) inhibitors allosterically control GTP affinity and effector interactions. *Nature* 503:548-551.
18. Hocker HJ, Cho KJ, Chen CY, Rambahal N, Sagineedu SR, Shaari K, Stanslas J, Hancock JF, Gorfe AA (2013) Andrographolide derivatives inhibit guanine nucleotide exchange and abrogate oncogenic Ras function. *Proc Natl Acad Sci USA* 110:10201-10206.
19. Shima F, Yoshikawa Y, Ye M, Araki M, Matsumoto S, Liao J, Hu L, Sugimoto T, Ijiri Y, Takeda A, Nishiyama Y, Sato C, Muraoka S, Tamura A, Osoda T,Tsuda K, Miyakawa T, Fukunishi H, Shimada J, Kumasaka T, Yamamoto M, Kataoka T (2013) In silico discovery of small molecule Ras inhibitors that display antitumor activity by blocking the Ras-effector interaction. *Proc Natl Acad Sci USA* 110:8182-8187.
20. Roskoski R Jr (2010) RAF protein-serine/threonine kinases: structure and regulation. *Biochem Biophys Res Commun* 399:313-317.
21. Mott HR, Owen D (2015) Structures of Ras superfamily effector complexes: What have we learnt in two decades? *Crit Rev Biochem Mol Biol* 50: 85-133.
22. Fetics SK, Guterres H, Kearney BM, Buhrman G, Ma B, Nussinov R, Matthos C (2015) Allosteric effects of the oncogenic RasQ61L mutant on Raf-RBD. *Structure* 23:505-516.
23. Aramini JM, Vorobiev SM, Tuberty LM, Janjua H, Campbell ET, Seetharaman J, Su M, Huang YJ, Acton TB, Xiao R, Tong L, Montelione GT (2015) The RAS-binding domain of human BRAF protein serine/threonine kinase exhibits allosteric conformational changes upon binding HRAS. *Structure* 23:1382-1393.
24. Brtva TR, Drugan JK, Ghosh S, Terrell RS, Campbell S, Bell RM, Der CJ (1995) Two distinct Raf domains mediate interaction with Ras. *J Biol Chem* 270: 9809-9812.
25. Clark GJ, Drugan JK, Terrell RS, Bradham C, Der CJ, Bell RM, Campbell S (1996) Peptides containing a consensus Ras binding sequence from Raf-1 and the GTPase activating protein NF1 inhibit Ras function. *Proc Natl Acad Sci USA* 93:1577-1581.
26. Mott HR, Carpenter JW, Zhong S, Ghosh S, Bell RM, Campbell SL (1996) The solution structure of the Raf-1 cysteine-rich domain: a novel ras and phospholipid binding site. *Proc Natl Acad Sci USA* 93: 8312-8317.
27. Improta-Brears T, Ghosh SF, Bell RM (1999) Mutational analysis of Raf-1 cysteine rich domain: requirement for a cluster of basic aminoacids for interaction with phosphatidylserine. *Mol Cell Biochem* 198:171–178.
28. Hekman M, Hamm H, Villar AV, Bader B, Kuhlmann J, Nickel J, Rapp UR (2002) Associations of B- and C-Raf with cholesterol, phosphatidylserine, and lipid second messengers: preferential binding of Raf to artificial lipid rafts. *J Biol Chem* 277: 24090-24102.
29. Zhou Y, Prakash P, Liang H, Cho KJ, Gorfe AA, Hancock JF (2017) Lipid-sorting specificity encoded in K-Ras membrane anchor regulates signal output. *Cell* 168:239-251.
30. Weise K, Kapoor S, Denter M, Nikolaus J, Opitz N, Koch S, Triola G, Herrmann A, Waldmann H, Winter R (2011) Membrane-mediated induction and sorting of K-Ras microdomain signaling platforms. *J Am Chem Soc* 133:880-887.
31. Abankwa D, Gorfe AA, Inder K, Hancock JF (2010) Ras membrane orientation and nanodomain localization generate isoform diversity. *Proc Natl Acad Sci USA* 107:1130-1135.
32. Prakash P, Zhou Y, Liang H, Hancock JF, Gorfe AA (2016) Oncogenic K-RAS binds to an anionic membrane in two distinct orientations: a molecular dynamics simulations. *Biophys J* 110:1125-1138.
33. Li ZL, Buck M (2017) Computational modeling reveals that signaling lipids modulate the orientation of K-Ras4A at the membrane reflecting protein topology. *Structure* 25:679-689.
34. Kapoor S, Weise K, Erlkamp M, Triola G, Waldmann H, Winter R (2012) The role of G-domain orientation and nucleotide state on the Ras isoform-specific membrane interaction. *Eur Biophys J* 41:801-813.
35. Pham E, Chiang J, Li I, Shum W, Truong K (2007) A computational tool for designing FRET protein biosensors by rigid-body sampling of their conformational space. *Structure* 15:515-523.
36. Thapar R, Williams JG, Campbell SL (2004) NMR characterization of full-length farnesylated and non-farnesylated H-Ras and its implications for Raf activation. *J Mol Biol* 343:1391-408.
37. Gorfe AA, Grant BJ, McCammon JA (2008) Mapping the nucleotide and isoform-dependent structural and dynamical features of Ras proteins. *Structure* 16:885-896.
38. Lomize MA, Lomize AL, Pogozheva ID, Mosberg HI (2006) OPM: Orientations of Proteins in Membranes database. *Bioinformatics* 22:623-625.

39. Buck M, Xu W, Rosen MK (2004) A two-state allosteric model for autoinhibition rationalizes WASP signal integration and targeting. *J Mol Biol* 338:271-285.
40. Dueber JE, Yeh BJ, Chak K, Lim WA (2003) Reprogramming control of an allosteric signaling switch through modular recombination. *Science* 301:1904-1908.
41. Prakash P, Gorfe AA (2016) Membrane orientation dynamics of lipid-modified small GTPases. *Small GTPases* Aug 11:1-10.
42. Muratcioglu S, Chavan TS, Freed BC, Jang H, Khavrutskii L, Freed RN, Dyba MA, Stefanisko K, Tarasov SG, Gursoy A, Keskin O, Tarasova NI, Gaponenko V, Nussinov R (2015) GTP-dependent K-Ras dimerization. *Structure* 23:1325-1335.
43. Prakash P, Sayyed-Ahmad A, Cho KJ, Dolino DM, Chen W, Li H, Grant BJ, Hancock JF, Gorfe AA (2017) Computational and biochemical characterization of two partially overlapping interfaces and multiple weak-affinity K-Ras dimers. *Sci Rep* 7:40109.
44. Cutler RE, Stephens RM, Saracino, MR, Morrison, DK (1998) Autoregulation of the Raf-1 serine/threonine kinase. *Proc Natl Acad Sci USA* 95: 9214–9219.
45. Zalatan JG1, Coyle SM, Rajan S, Sidhu SS, Lim WA (2012) Conformational control of the Ste5 scaffold protein insulates against MAP kinase misactivation. *Science* 337:1218-1222.
46. Herzog FA, Braun L, Schoen I, Vogel V (2017) Structural insights how PIP2 imposes preferred binding orientations of FAK at lipid membranes. *J Phys Chem B* 121:3523-3535.
47. Liang FC, Kroon G, McAvoy CZ, Chi C, Wright PE, Shan SO (2016) Conformational dynamics of a membrane protein chaperone enables spatially regulated substrate capture and release. *Proc Natl Acad Sci USA* 113:E1615-E1624.
48. Hancock WO (2014) Bidirectional cargo transport: moving beyond tug of war. *Nat Rev Mol Cell Biol* 15:615-628.
49. Huang J, Rauscher S, Nawrocki G, Ran T, Feig M, de Groot BL, Grubmüller H, MacKerell AD (2017) CHARMM36m: an improved force field for folded and intrinsically disordered proteins. *Nat Methods* 14:71-73.
50. Xu D, Jaroszewski L, Li Z, Godzik A (2014) AIDA: ab initio domain assembly server. *Nucleic Acids Res* 42: W308–W313.
51. Godwin RC, Melvin RL, Gmeiner WH, Salsbury FR (2017) Binding Site Configurations Probe the Structure and Dynamics of the Zinc Finger of NEMO (NF-κB Essential Modulator). *Biochemistry* 56: 623-633.
52. Vanommeslaeghe K, Mackerell AD (2012) Automation of the CHARMM general force field (CGenFF) I: bond perception and atom typing. *J Chem Inf Model* 52:3144-3154.
53. Wu EL, Cheng X, Jo S, Rui H, Song KC, Davila-Contreras EM, Qi Y, Lee J, Monje-Galvan V, Venable RM, Klauda JB, Im W (2014) CHARMM-GUI membrane builder toward realistic biological membrane simulations. *J Comput Chem* 35:1997-2004.
54. Phillips JC, Braun R, Wang W, Gumbart J, Tajkhorshid E, Villa E, Chipot C, Skeel RD, Kale L, Schultern K (2005) Scalable molecular dynamics with NAMD. *J Comput Chem* 26:1781-1802.
55. Shaw, DE, Grossman JP, Bank JA, Batson B, Butts JA, Chao JC, Deneroff MM (214) Anton 2: Raising the bar for performance and programmability in a special-purpose molecular dynamics supercomputer. *IEEE* 41-53.
56. Roux B (1995) The calculation of the potential of mean force using computer simulations. *Comput Phys Commun* 91: 275-282.
57. Kumar S, Bouzida D, Swendsen RH, Kollman PA, Rosenberg JM (1992) The weighted histogram analysis method for free-energy calculations on biomolecules. I. The method. *J Comput Chem* 13:1011–1021.
58. Seeber M, Cecchini M, Rao F, Settanni G, Caflisch A (2007) Wordom: a program for efficient analysis of molecular dynamics simulations. *Bioinformatics* 23:2625-2627.